Sensors & Actuators: B. Chemical 284 (2019) 140–147

Contents lists available at ScienceDirect

Sensors and Actuators B: Chemical

journal homepage: www.elsevier.com/locate/snb

Highly sensitive metal-enhanced fluorescence biosensor prepared on electrospun fibers decorated with silica-coated silver nanoparticles

Byung Ju Yun[a,b], Ji Eon Kwon[c], Kangwon Lee[d,e,**], Won-Gun Koh[a,*]

[a] Department of Chemical and Biomolecular Engineering, Yonsei University, Seoul, Republic of Korea
[b] Next-Generation Converged Energy Material Research Center, Seoul, Republic of Korea
[c] Research Institute of Advanced Materials (RIAM), Seoul National University, Seoul, Republic of Korea
[d] Program in Nanoscience and Technology, Graduate School of Convergence Science and Technology, Seoul National University, Seoul, Republic of Korea
[e] Advanced Institutes of Convergence Technology, Gyeonggi-do, Republic of Korea

ARTICLE INFO

Keywords:
Metal-enhanced fluorescence
Fibrous substrates
Silver-decorated fibers
Silica layer
Fluorescence-based immunoassay

ABSTRACT

A new metal-enhanced fluorescence (MEF)-based biosensor platform was prepared on fibrous substrates. First, polycaprolactone (PCL) fibers were obtained via electrospinning process. PCL fibers were decorated with photoreduced silver nanoparticles followed by silica coating, generating silver-decorated PCL fibers with a silica layer (Ag@SiO_2-PCL). The silica layer acted as a spacer between the silver nanoparticles and the fluorescent molecules to optimize the MEF effect. The MEF was obtained from the silver-decorated PCL fibers, the extent of which could be controlled by the thickness of the silica layer. The fibrous structure of Ag@SiO_2-PCL had higher protein loading capacity than conventional two-dimensional glass slides due to its large surface area, while the presence of silica-coated silver nanoparticles resulted in higher fluorescence intensity than silica-coated PCL fibers (SiO_2-PCL) without silver nanoparticles via the MEF effect. Both features of Ag@SiO_2-PCL were combined to produce combined effects in improving the performance of fluorescence-based biosensing. According to immunobinding assays between fluorescently labeled anti-IgG and IgG immobilized onto different substrates, Ag@SiO_2-PCL had much better sensing performance in terms of sensitivity and detection limit than glass slides and SiO_2-PCL due to the combined effects of a large surface area and the MEF effect.

1. Introduction

There have been strong demands for fluorescence-based biosensor to improve the performance of biosensors as well as to increase sensitivity [1]. Generally, the substrate used for fluorescence-based assays consists of a two-dimensional flat substrate such as a silicon wafer or a glass slide, which makes it difficult to immobilize large amounts of biomolecules; thus, the overall assay performance is very low [2,3]. New biosensor platforms have been developed by incorporating various nano- or microstructures such as printed patterns, particles, and tubes to overcome this limitation of conventional 2D substrates [4–6]. Nevertheless, these nanostructures still have many problems that need to be addressed since the fabrication process is complex and requires a large investment of time and money [7]. Recently, electrospinning-based nano/micro fibrous substrates have emerged as a new alternative substrate for fluorescence-based bioassays because electrospinning can produce a loosely connected fibrous three-dimensional (3D) substrate with a large surface area in a relatively simple manner at low cost [8,9]. Electrospun fibers were also obtained as free-standing and bi-directionally porous structure, which allows for the easy handling of substrates and fast diffusion of target molecules [10,11].

On the other hands, there have been efforts to enhance the fluorescence emission at the interface using surface plasmon from metal or photonic crystals [12,13]. For example, metal-enhanced fluorescence (MEF)-based methods are applied to biosensor system to enhance the sensitivity of fluorescence-based detection [14–16]. The MEF effect is a

Abbreviations: MEF, metal-enhanced fluorescence; PCL, polycaprolactone; TFE, 2,2,2-trifluoroethanol; TEOS, tetraethyl orthosilicate; BSA, bovine serum albumin; APTES, 3-aminopropyltriethoxysilane; FITC, fluorescein isocyanate; PBS, phosphate buffered saline; SEM, scanning electron microscopy; TEM, transmission electron microscopy; AFM, atomic force microscopy; XPS, x-ray photoelectron spectroscopy; TCSPC, time correlated single photon counting; IRF, instrumental response function

* Corresponding author.
** Corresponding author at: Program in Nanoscience and Technology, Graduate School of Convergence Science and Technology, Seoul National University, Seoul, Republic of Korea.
E-mail addresses: kangwonlee@snu.ac.kr (K. Lee), wongun@yonsei.ac.kr (W.-G. Koh).

https://doi.org/10.1016/j.snb.2018.12.096
Received 9 September 2018; Received in revised form 14 December 2018; Accepted 19 December 2018
Available online 21 December 2018

phenomenon in which emission intensity of a fluorophore increases due to electromagnetic interaction between a fluorophore and the surface of metal nanoparticles such as gold and silver [17]. When a specific wavelength of light is irradiated with a specific distance between fluorophores and metal nanoparticles, a strong excitation field is generated by the surface plasmon of the metal nanoparticles, and this energy is transferred to fluorophores to increase their emission rate [18]. Most MEF-based biosensor systems use one of two general platforms. The first is a two-dimensional (2D) planar MEF platform where metal nanopatterns or nanoparticles are deposited on flat substrates [19,20] and the second is a suspension MEF platform where metallic colloids are dispersed in solution [21–23]. Since the distance between metal and fluorescence materials is very important to optimize the MEF effect, both systems have inorganic or organic spacers that are coated onto metal nanostructures [24]. Various types and shapes of metal nanostructures have also been investigated to maximize the MEF effect [25].

In this study, we proposed new highly sensitive fluorescence-based biosensor platform that combined the advantages of both fiber substrates and the MEF effect. Silver nanoparticle-decorated, electrospun fibrous substrates were developed for the new MEF-based biosensor, where the fluorescence intensity of protein-conjugated fluorophore was significantly enhanced by the combined effects of a large surface to volume ratio of fibrous matrix and the MEF from the silver nanoparticles. The MEF effect was optimized by depositing a silica layer as a spacer onto the silver-decorated fibers. After confirming the MEF effect from the resultant fibrous substrates, immunoassays using IgG and fluorescence-labeled anti IgG were carried out, and the sensitivity of the assay was compared with 2D substrates and fibrous substrates without MEF.

2. Experimental

2.1. Materials

Polycaprolactone (PCL, MW 80,000), 2,2,2-trifluoroethanol (TFE, CF_3CH_2OH), ammonium hydroxide solution (NH_4OH, 28.0–30.0 %), tetraethyl orthosilicate (TEOS), silver nitrate ($AgNO_3$), bovine serum albumin (BSA), 3-aminopropyltriethoxysilane (APTES), and BSA-conjugated with fluorescein isocyanate (FITC-BSA) were purchased from Sigma-Aldrich (Milwaukee, WI, USA). Glutaraldehyde (25% solution) was purchased from Junsei Chemical (Tokyo, Japan). Phosphate buffered saline (PBS, 0.1 M, pH 7.4) was purchased from Invitrogen Corp. (Carlsbad, CA, USA). Pierce® BCA Protein Assay Kit was purchased from Pierce (Rockford, IL, USA). Mouse IgG and FITC-rabbit anti-mouse IgG (FITC-anti IgG) were purchased from ZYMED Laboratories (San Francisco, CA, USA).

2.2. Fabrication of different fibrous substrates

PCL was dissolved in TFE at 20 wt %. This solution was kept in a convection oven for one day and then moved to a syringe. A voltage of 10 kV was applied, and the solution was fed at a flow velocity of 0.6 mL/h to conduct the electrospinning. Aluminum foil was located at a distance of 20 cm from the tip of syringe needle and PCL fibers were collected on it for 30 min. After 10 min of oxygen plasma treatment (Femto Science, Kyunggi, Korea) with a radio frequency power of 100 W and a pressure of 0.1 mmHg, PCL fibers were immersed in $AgNO_3$ solution (100 mM) for 30 min. Then, the PCL fibers were exposed to UV light (365 nm, 300 mW cm^{-2}) for 10 min, generating silver-decorated PCL fibers (Ag-PCL). A silica layer was coated onto the surface of Ag-PCL by the hydrolysis and condensation of TEOS through the Stöber process. Briefly, different amounts of TEOS (10, 30, 50, and 70 μL) were added to the 5 mL of ethanol solution containing Ag-PCL while vigorously stirring and then, 500 μL NH_4OH was added to the solution while continuously stirring for 2 h. The silver-decorated PCL fibers with silica layer were expressed as Ag@SiO_2-PCL. For the evaluation of MEF effect, silica-coated PCL fibers without silver nanoparticles (SiO_2-PCL) was prepared using 30 μL of TEOS as a control sample.

2.3. Protein immobilization and immunoassay

The 0.7 cm × 0.7 cm of glass slide, Silica-coated PCL fibers (SiO_2-PCL), and Ag@SiO_2-PCL were oxidized in oxygen plasma for 10 min. Each substrate was silanized in a 0.05% (v/v) solution of APTES in ethanol for 1 h under vacuum conditions and then washed with ethanol. APTES-treated substrates were immersed in a 2.5% (v/v) solution of glutaraldehyde in PBS for 2 h to activate the amine groups of APTES and rinsed with deionized water. Then, each substrate was reacted with either 10 μg/mL of FITC-BSA or 25 μg/mL of mouse IgG solution for 2 h. Glutaraldehyde chemically binds the amine groups of APTES and proteins (BSA or IgG) through an imine bonds. The amount of proteins immobilized onto different substrates was measured using a BCA protein assay kit, as described in our previous study [26]. For immunoassay, IgG-immobilized substrates were blocked with BSA solution (1 wt% BSA in PBS solution) to prevent non-specific adsorption and were exposed to different concentrations of FITC-anti IgG for 2 h.

2.4. Material characterization

The morphology of different fibrous substrates was observed using scanning electron microscopy (SEM) (JSM-7001 F, JEOL Ltd., Japan), transmission electron microscope (TEM) (Philips Electron Optics, Netherlands), and atomic force microscopy (AFM) measurements (Dimension 3100/Nanoscope Iva, Digital Instruments, Santa Barbara, CA, USA). The RMS roughness value of three kinds of fibers sheet was calculated from AFM analysis using Gwyddion SPM data analysis software. The chemical properties of PCL fibers, Ag-PCL, and Ag@SiO_2-PCL were analyzed using X-ray photoelectron spectroscopy (XPS, K-alpha, Thermo, UK). The porosity and pore size of PCL fibers and Ag@SiO_2-PCL were obtained by using porosimeter (Quantachrome Inst, PM33GT, Boynton Beach, FL, USA).

2.5. Fluorescence characterization

Fluorescence images were obtained by a Zeiss Axiovert 200 microscope installed with an integrated color CCD camera (Carl Zeiss Inc., Thornwood, NY, USA). The 488-nm excitation/green emission filter (dichroic mirror 488/568/647; bandpass 500–560) was used for FITC-conjugated protein detection. The fluorescence intensity from each substrate was calculated through image analysis software (KS 300, Carl Zeiss Inc.). The fluorescence intensity was obtained by excluding background signal values at a zero concentration of fluorescence-labeled proteins. The mean and standard deviation of fluorescence intensity values of the different substrates were obtained by averaging the intensities of six arbitrarily-chosen areas (100 μm × 100 μm) of each sample, where three samples from each substrate were used for one data point. The confocal fluorescence image from the Ag@SiO_2-PCL was observed with a confocal laser scanning microscope (LSM 700, Carl Zeiss, Oberkochen, Germany). Time-resolved fluorescence lifetime measurements were carried out using the time-correlated single photon counting (TCSPC) method by using a FluoTime 200 instrument (Picoquant, Berlin, Germany). A 377 nm diode laser with a repetition rate of 5 MHz was used as an excitation source. Fluorescence decay profiles were analyzed with FluoFit Pro software using an exponential fitting model through deconvolution with the measured instrumental response function (IRF).

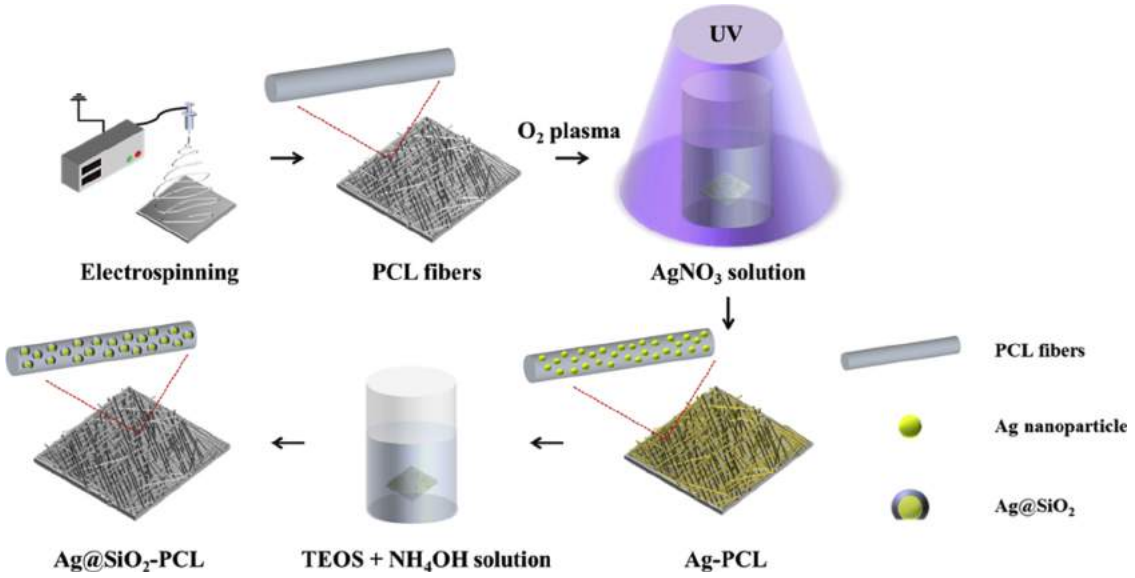

Fig. 1. The overall fabrication process of $Ag@SiO_2$-PCL.

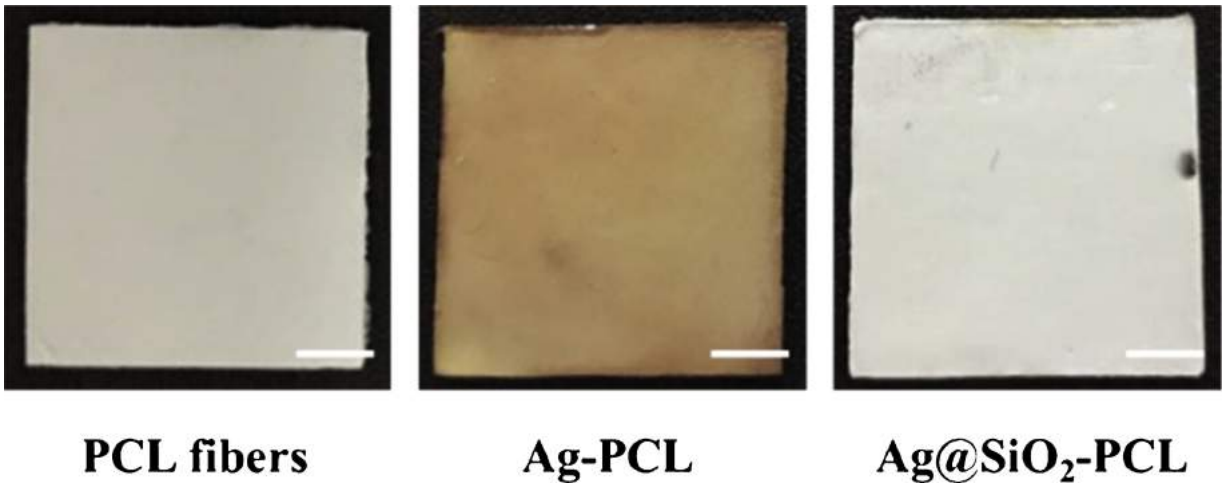

Fig. 2. Photograph of PCL fibers, Ag-PCL, and $Ag@SiO_2$-PCL. Scale bar: 1 cm.

3. Results and discussion

3.1. Fabrication of $Ag@SiO_2$-PCL

The fibers-based MEF platform, $Ag@SiO_2$-PCL, was prepared through three steps as described in Fig. 1. First, randomly-oriented PCL fibrous matrixes were obtained via an electrospinning process. The diameter of the fibers was 1.95 ± 0.18 μm, and the thickness of the matrix was approximately 25 μm. The porosity and average pore size of the PCL fibrous matrix were 63.6% and 4.3 μm, respectively, which were large enough to enable the free diffusion of probe and target proteins throughout the fibrous matrix. Next, electrospun fibers were plasma-treated and immersed in $AgNO_3$ solution. The subsequent photoreduction reaction via UV exposure generated silver nanoparticles on the surface of the PCL fibers. A plasma treatment produced hydroxyl groups on the surface of the hydrophobic PCL fibers to make them hydrophilic and react easily with $AgNO_3$ solution [27,28]. The negatively-charged hydroxyl groups had electrostatic interactions with Ag^+ to form a complex that facilitated Ag^+ to Ag nanoparticles via an UV-initiated photoreduction [29]. Finally, silica layers were formed on the surface of Ag-PCL via the Stöber process [30]. Although the thickness of the silica layer increased with the amount of TEOS, this increase in thickness was not large enough to significantly change the porosity of the fibrous matrix. The porosity of $Ag@SiO_2$-PCL prepared from 70 μL TEOS (the largest amount of TEOS used in this study) was 62.3%. Fig. 2 shows the photographs of three different fibers-based substrates. The white bare PCL fibers became brown color due to the surface plasmon absorbance of the silver nanoparticles [31]. The color of fibers-based substrates returned to white after a deposition of a silica layer.

3.2. Characterization of $Ag@SiO_2$-PCL

The surface morphology of different fiber substrates was assessed by SEM, TEM and AFM (Fig. 3). The SEM images shown in Fig. 3a revealed that the bare PCL fibers had a smooth surface. In contrast, silver nanoparticles were shown on the surface of the PCL fibers in the Ag-PCL sample after photoreduction. In the case of $Ag@SiO_2$-PCL, relatively large silica nanoparticle layers were observed, and they covered the whole surface of silver nanoparticles and PCL fibers. TEM image shown in Fig. 3b confirmed the synthesis of 30–50 nm silver nanoparticles and subsequent formation of silica layer on the Ag-PCL. (Fig. 3b). The thickness of silica layer increased from 15.5 to 28.3, 56.1, and 89.4 nm as the amount of TEOS increased from 10 to 30, 50, and 70 μL as shown in Fig. 3c. The images obtained through the AFM analysis showed a

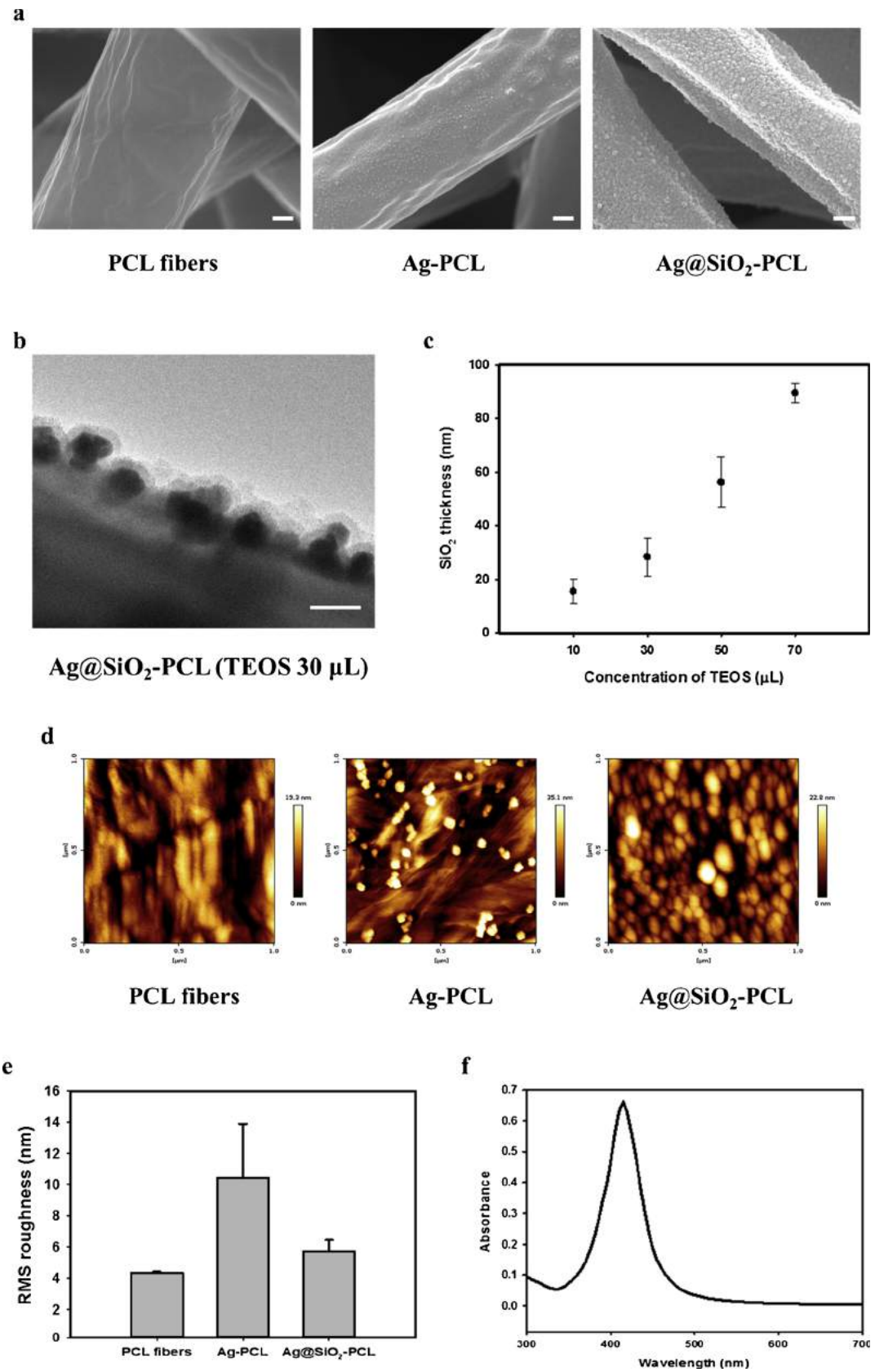

Fig. 3. Surface morphology characterization of different fibrous substrates. (a) SEM images. (b) TEM image of Ag@SiO_2-PCL (TEOS 30 µL). (c) Range of silica layer thickness according to TEOS concentration. (d) AFM images. (e) resultant RMS roughness values. (f) Absorbance spectra of silver nanoparticles on PCL fibers. Scale bar: 300 nm in (a) and 50 nm in (b).

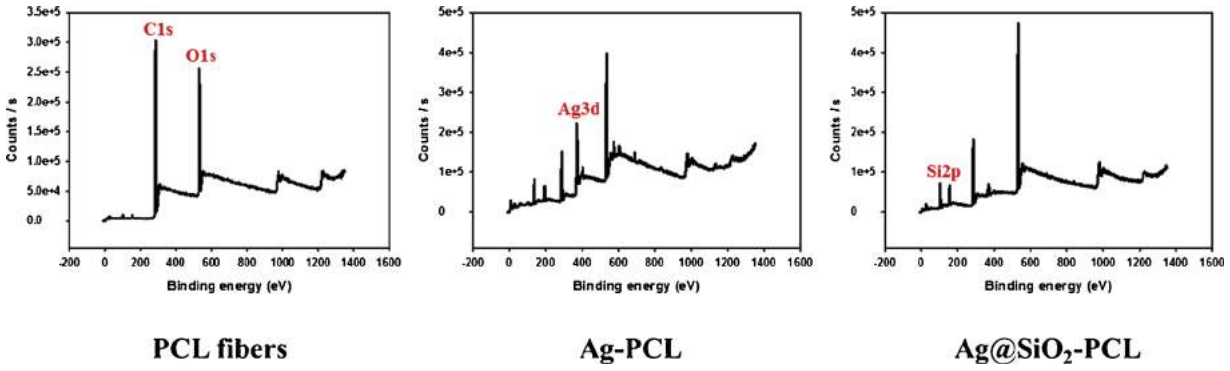

Fig. 4. XPS spectra of PCL fibers, Ag-PCL, and Ag@SiO_2-PCL.

similar pattern as the SEM images. AFM images confirmed the formation of approximately silver nanoparticles and layer of larger silica nanoparticles on the surface of the PCL fibers, while the bare PCL fibers had a smooth surface (Fig. 3d). The RMS roughness (R_q) values were also obtained through AFM analysis. The R_q of the Ag-PCL was significantly higher than of the PCL fibers due to the presence of the silver nanoparticles. On the other hand, the R_q of the Ag@SiO_2-PCL in which the layer of silica nanoparticles was uniformly distributed on the surface of the fibers was found to be significantly reduced compared to the Ag-PCL (Fig. 3e). Fig. 3f shows that Ag@SiO_2-PCL had distinct, characteristic absorption peaks at approximately 420 nm, which arises from the surface plasmon absorbance of silver nanoparticles on the PCL fibers.

The formation of silver nanoparticles and silica layers on the PCL fibers was further verified using XPS. Fig. 4 shows the XPS spectra obtained from three different fiber substrates (PCL fibers, Ag-PCL, and Ag@SiO_2-PCL). Bare PCL fibers have only C1s and O1s peaks at 280˜290 eV and 530˜535 eV, respectively, while new Ag3d peak at 360˜380 eV and Si2p peak at 99˜100 eV appeared after decoration with silver nanoparticles and deposition of the silica layers. Combining the results of the morphology and chemical analysis, we can confirm that new MEF substrates based on Ag@SiO_2-PCL were successfully fabricated through sequential steps consisting of electrospinning, photoreduction and the Stöber process.

3.3. Verification of MEF effect via protein immobilization

Next, we investigated the possibility that Ag@SiO_2-PCL could be applied to a MEF-based highly sensitive biosensor platform. In this paper, two-dimensional (2D) glass slides and SiO_2-PCL were used as control substrates for comparison. First, FITC-BSA was covalently immobilized onto three different substrates using APTES as a conjugation linker to compare the protein loading capacity between different substrates and to determine the presence of the MEF effect from the Ag@SiO_2 layer. APTES provided amine groups on each substrate, which were converted to aldehyde groups by glutaraldehyde treatment and formed stable imine bonds with the amine groups of the proteins [32]. As shown in Fig. 5a, fluorescence intensity increased in the following order; 2D glass < SiO_2-PCL < Ag@SiO_2-PCL. The fluorescence intensity of Ag-PCL without the silica layer was significantly decreased by the fluorescence quenching effect, compared with that of the SiO_2-PCL. In the case of Ag@SiO_2-PCL, fluorescence intensity had different values depending on the amount of TEOS, that is, the thickness of the silica layer. This is because the MEF effect is significantly affected by the specific distance between the metal nanostructures and the fluorescent molecules. If the specific distance is too close, the quenching effect dominates. Therefore, fluorescence intensity from Ag-PCL without a silica layer was lower than that from the SiO_2-PCL. On the other hands, if the distance is too far, the MEF effect does not appear. Here, silica layers play two roles in the MEF platform. One is a coating layer for easy functionalization with APTES to covalently immobilize proteins and the other is a spacer for controlling the separation distance between metal and fluorophore to obtain the optimal MEF effect. The fluorescence intensity from Ag@SiO_2-PCL reached a maximum value at 30 μL of TEOS, which was 50.7 and 3.1 fold higher than those of the 2D glass and the SiO_2-PCL, respectively. The representative fluorescence images from four different substrates (Fig. 5b) were consistent with the fluorescence intensity data shown in Fig. 5a. Fig. 5c shows the actual amount of immobilized BSA per unit area on each substrate. The amount of BSA immobilized on the 3D fibrous substrates was found to be significantly higher than that of 2D glass because of large surface area of fiber matrix. However, the amount of immobilized BSA was almost same between different fiber substrates regardless of the presence of an Ag@SiO_2 layer or the thickness of silica layers. An analysis in connection with the previous results (Fig. 5a and 5b) indicates that the difference in fluorescence intensity between the 2D glass and the fibrous substrates (SiO_2-PCL and Ag@SiO_2-PCL) was mainly due to the difference in the amount of immobilized BSA, while the difference between the SiO_2-PCL and the Ag@SiO_2-PCL was due to the presence of MEF. Therefore, a highly sensitive fluorescence-based biosensor can be developed from Ag@SiO_2-PCL via the combined effects of a large surface area of electrospun fibers and MEF from Ag@SiO_2 decorated on the fibers. The fluorescence intensity profile (Fig. 5d) proves that the fluorescence intensity of Ag@SiO_2-PCL was almost the same at all points. This result indicates that Ag@SiO_2 and FITC-BSA were evenly distributed on the fibrous substrate. The fluorescence lifetimes of the SiO_2-PCL and Ag@SiO_2-PCL immobilizing FITC-BSA were obtained as shown in Fig. 5e. The fluorescence decay curves confirmed that the average fluorescence lifetime of Ag@SiO_2-PCL was reduced compared to the SiO_2-PCL (2.91 ns → 2.12 ns), which indirectly demonstrated the MEF effect [33]. In addition, the fitting curves were derived, and chi-squared values from SiO_2-PCL and Ag@SiO_2-PCLwere obtained to confirm the goodness of fitting, which were 1.138 and 0.964, respectively. Generally, the closer the chi-squared value is to 1, the better the fitting.

3.4. Immunoassays

Finally, we investigated the suitability of the Ag@SiO_2-PCL to the immunoassay platform by reacting FITC-anti IgG with IgG immobilized onto different substrates. Fig. 6a shows the fluorescence intensities from 2D glass, SiO_2-PCL, and Ag@SiO_2-PCL after reacting FITC-anti IgG with IgG immobilized onto the substrates. Similar to the FITC-BSA experiment results, the fluorescence intensity of the Ag@SiO_2-PCL was significantly higher (42.5 fold) than that of the 2D glass due to a higher IgG loading capacity. The use of the Ag@SiO_2-PCL further enhanced fluorescence intensity that was 3.4 fold higher than from the SiO_2-PCL due to the MEF effect. Also, It is noteworthy that maximum fluorescence intensity was obtained when 10 μL of TEOS was used, which was a smaller amount than the FITC-BSA experiment. This result indicates

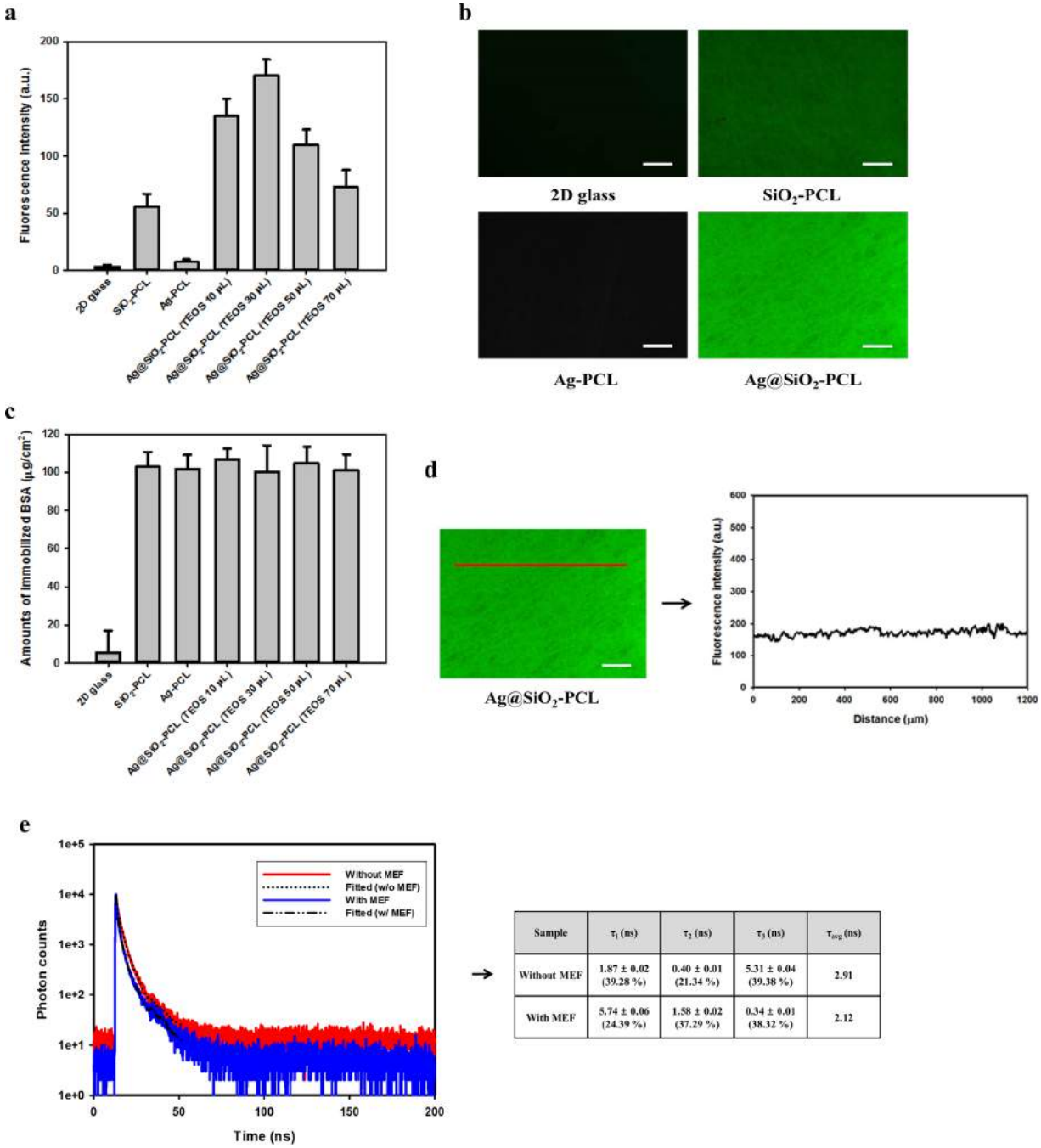

Sample	τ_1 (ns)	τ_2 (ns)	τ_3 (ns)	τ_{avg} (ns)
Without MEF	1.87 ± 0.02 (39.28 %)	0.40 ± 0.01 (21.34 %)	5.31 ± 0.04 (39.38 %)	2.91
With MEF	5.74 ± 0.06 (24.39 %)	1.58 ± 0.02 (37.29 %)	0.34 ± 0.01 (38.32 %)	2.12

Fig. 5. Immobilization of FITC-BSA on the different substrates. All the substrates were incubated with the same concentration of FITC-BSA (10 μg/mL). (a) Fluorescence intensities obtained from different substrates. (b) Fluorescence images. (c) The actual amount of BSA immobilized on each substrate. (d) Fluorescence intensity profile over different region in Ag@SiO_2-PCL. (e) Fluorescence decay curves and fluorescence lifetime measurement of SiO_2-PCL and Ag@SiO_2-PCL immobilizing FITC-BSA. For fluorescence image, intensity profile and lifetime measurement of Ag@SiO_2-PCL, TEOS 30 μL sample were used. Scale bar: 200 μm.

that a thinner silica spacer is necessary to maximize the MEF effect in this immunoassay since immobilized IgG acted as an additional spacer between the silver nanoparticles and FITC, compared with a direct immobilization of FITC-BSA. When the silica layer became thicker than the optimal condition, fluorescence intensity approached to the same value as with SiO_2-PCL because the distance between the FITC and the silver nanoparticles is so long that the MEF effect cannot be reached. Fig. 6b shows the change in fluorescence intensity according to the FITC-anti IgG concentrations. All the substrates show the concentration-dependent fluorescence intensity but a significantly higher sensitivity, (Δ fluorescence intensity)/(Δ concentration of anti IgG), was observed from Ag@SiO_2-PCL than the other substrates (26.8 and 2.4 fold higher than 2D glass and SiO_2-PCL, respectively). Under the same condition, the detection limit of Ag@SiO_2-PCL, SiO_2-PCL, and 2D glass were measured as 1.5, 25, and 530 ng/mL, respectively. The limit of detection (LOD) was determined by following equation [34], "LOD = 3.3 × SD/b", where SD is standard deviation of the blank sample and b is the slope of the regression line. Fig. 6c shows the confocal image and intensity profile obtained from Ag@SiO_2-PCL reacted with FITC-anti IgG. The fluorescence image obtained by setting three z-axis points (each was 8, 17, 24 μm, from the top of the fibrous substrate) on any cross-section had almost the same intensity profiles. This result reveals that fibrous networks were porous enough to allow the free diffusion of FITC-anti IgG through the fiber matrix so that similar fluorescence

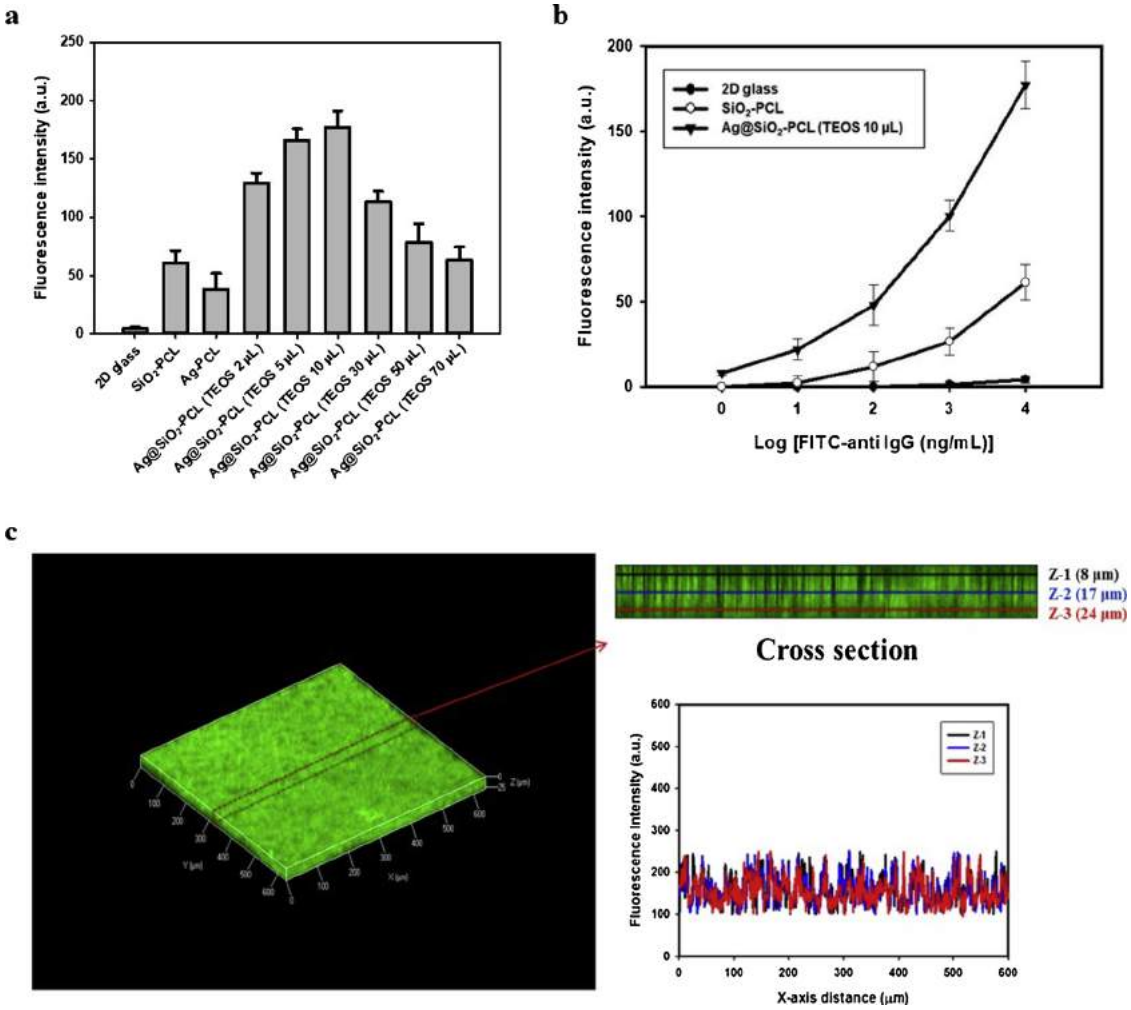

Fig. 6. Immunoassays result from the reaction between FITC-anti IgG and substrate-immobilized IgG. (a) Fluorescence intensity obtained from different substrates that reacted with 10 μg/mL FITC-anti IgG. (b) Change of fluorescence intensities as a function of FITC-anti IgG concentration. (c) Confocal image and fluorescence intensity profile of Ag@SiO_2-PCL reacted with FITC-anti IgG. Ag@SiO_2-PCL (TEOS 10 μL) was used.

Table 1
Performance comparison of immunoassay between IgG and anti-IgG that used silver-containing substrates.

Substrate	Detection method	Detection limit	Incubation time	Reference
PDA-AgNPs-PDA-Au film	SPR	0.625 μg mL^{-1}	Not reported	[35]
AgNPs film	MEF	50 ng mL^{-1}	1 h	[36]
AgNPs multilayer films	MEF	Not reported	2 h	[37]
Monolayer protected Ag film	SPR	22.516 ng mL^{-1}	40 min	[38]
Graphene oxide/Ag coated polymer cladding silica fiber	SPR	40 ng mL^{-1}	70 min	[39]
Au/Ag alloy nanocomposites	SPR	0.15 μg mL^{-1}	Not reported	[40]
Ag@SiO_2-PCL fibers	MEF	1.5 ng mL^{-1}	2 h	This study

intensities were observed from different positions in the z-axis of the Ag@SiO_2-PCL cross-section. Finally, we summarized previous results for immunoassays between IgG and anti-IgG that used silver-containing substrates (Table 1). With the help of combined effect of MEF and fibrous substrates, it was possible to develop the immunoassay with better performance than previously-reported system.

4. Conclusion

In this study, we fabricated fibrous Ag@SiO_2-PCL substrates as a novel MEF-based biosensor platform, which was produced by a sequential process of electrospinning, photoreduction, and the Stöber process. The MEF phenomenon appeared via silver nanoparticles and was optimized by a silica layer that was used as a spacer between the silver nanoparticles and the fluorescent molecules in fibrous substrates. Ag@SiO_2-PCL significantly increased the fluorescence intensity of protein-conjugated fluorophores through a combined effect of a large surface to volume ratio of the fibrous matrix and MEF from silica-coated silver nanoparticles. Therefore, immunoassays using IgG and FITC-anti IgG on the Ag@SiO_2-PCL emitted enhanced fluorescence signals and had higher sensitivity than assays carried out on flat 2D glass slide and on SiO_2-PCL. We believe that the MEF effect can be further improved by controlling the type, size and shape of the metal-based nanostructures dispersed on the fibers. Furthermore, a fiber-based MEF platform can be combined with a microarray and microfluidic system for highly sensitive and high-throughput bioassays.

Acknowledgments

This work was supported by the National Research Foundation (NRF) grant funded by the Ministry of Science and ICT (MSIT) (NRF-2017M3A7B4049848, NRF-2017M3D1A1039289 and 2017M3A7B4041798)

References

[1] J.C. Pickup, F. Hussain, N.D. Evans, O.J. Rolinski, D.J. Birch, Fluorescence-based glucose sensors, Biosens. Bioelectron. 20 (2005) 2555–2565.
[2] Y. Lee, H.J. Lee, K.J. Son, W.-G. Koh, Fabrication of hydrogel-micropatterned nanofibers for highly sensitive microarray-based immunosensors having additional enzyme-based sensing capability, J. Mater. Chem. 21 (2011) 4476–4483.
[3] Y. Lee, S. Park, S.W. Han, T.G. Lim, W.-G. Koh, Preparation of photolithographically patterned inverse opal hydrogel microstructures and its application to protein patterning, Biosens. Bioelectron. 35 (2012) 243–250.
[4] J.-U. Park, J.H. Lee, U. Paik, Y. Lu, J.A. Rogers, Nanoscale patterns of oligonucleotides formed by electrohydrodynamic jet printing with applications in biosensing and nanomaterials assembly, Nano Lett. 8 (2008) 4210–4216.
[5] H. Aldewachi, T. Chalati, M.N. Woodroofe, N. Bricklebank, B. Sharrack, P. Gardiner, Gold nanoparticle-based colorimetric biosensors, Nanoscale 10 (2018) 18–33.
[6] W.-T. Chen, S.-S. Li, J.P. Chu, K.C. Feng, J.-K. Chen, Fabrication of ordered metallic glass nanotube arrays for label-free biosensing with diffractive reflectance, Biosens. Bioelectron. 102 (2018) 129–135.
[7] S. Zhang, R. Geryak, J. Geldmeier, S. Kim, V.V. Tsukruk, Synthesis, assembly, and applications of hybrid nanostructures for biosensing, Chem. Rev. 117 (2017) 12942–13038.
[8] D. Yang, X. Liu, Y. Jin, Y. Zhu, D. Zeng, X. Jiang, H. Ma, Electrospinning of poly (dimethylsiloxane)/poly (methyl methacrylate) nanofibrous membrane: fabrication and application in protein microarrays, Biomacromolecules 10 (2009) 3335–3340.
[9] D. Wu, D. Han, A.J. Steckl, Immunoassay on free-standing electrospun membranes, ACS Appl. Mater. Interfaces 2 (2009) 252–258.
[10] A. Senthamizhan, A. Celebioglu, B. Balusamy, T. Uyar, Immobilization of gold nanoclusters inside porous electrospun fibers for selective detection of Cu (II): a strategic approach to shielding pristine performance, Sci. Rep. 5 (2015) 15608.
[11] A.-F. Che, V. Germain, M. Cretin, D. Cornu, C. Innocent, S. Tingry, Fabrication of free-standing electrospun carbon nanofibers as efficient electrode materials for bioelectrocatalysis, New J. Chem. 35 (2011) 2848–2853.
[12] M. Bauch, K. Toma, M. Toma, Q. Zhang, J. Dostalek, Plasmon-enhanced fluorescence biosensors: a review, Plasmonics 9 (2014) 781–799.
[13] A. Sinibaldi, A. Fieramosca, N. Danz, P. Munzert, A. Occhicone, C. Barolo, F. Michelotti, Effects of reabsorption due to surface concentration in highly resonant photonic crystal fluorescence biosensors, J. Phys. Chem. C 122 (2018) 26281–26287.
[14] J. Liu, S. Li, V.R. Bhethanabotla, Integrating metal-enhanced fluorescence and surface acoustic waves for sensitive and rapid quantification of cancer biomarkers from real matrices, ACS Sens. 3 (2018) 222–229.
[15] N. Sui, L. Wang, T. Yan, F. Liu, J. Sui, Y. Jiang, J. Wan, M. Liu, W.W. Yu, Selective and sensitive biosensors based on metal-enhanced fluorescence, Sens. Actuators, B 202 (2014) 1148–1153.
[16] E. Matveeva, Z. Gryczynski, J. Malicka, I. Gryczynski, J.R. Lakowicz, Metal-enhanced fluorescence immunoassays using total internal reflection and silver island-coated surfaces, Anal. Biochem. 334 (2004) 303–311.
[17] J.R. Lakowicz, Radiative decay engineering 5: metal-enhanced fluorescence and plasmon emission, Anal. Biochem. 337 (2005) 171–194.
[18] K. Aslan, I. Gryczynski, J. Malicka, E. Matveeva, J.R. Lakowicz, C.D. Geddes, Metal-enhanced fluorescence: an emerging tool in biotechnology, Curr. Opin. Biotechnol. 16 (2005) 55–62.
[19] S. Dutta Choudhury, R. Badugu, K. Ray, J.R. Lakowicz, Silver–gold nanocomposite substrates for metal-enhanced fluorescence: ensemble and single-molecule spectroscopic studies, J. Phys. Chem. C 116 (2012) 5042–5048.
[20] J. Zhang, J.R. Lakowicz, A model for DNA detection by metal-enhanced fluorescence from immobilized silver nanoparticles on solid substrate, J. Phys. Chem. B 110 (2006) 2387–2392.
[21] L. Lu, Y. Qian, L. Wang, K. Ma, Y. Zhang, Metal-enhanced fluorescence-based core–shell Ag@SiO_2 nanoflares for affinity biosensing via target-induced structure switching of aptamer, ACS Appl. Mater. Interfaces 6 (2014) 1944–1950.
[22] Y. Pang, Z. Rong, J. Wang, R. Xiao, S. Wang, A fluorescent aptasensor for H5N1 influenza virus detection based-on the core–shell nanoparticles metal-enhanced fluorescence (MEF), Biosens. Bioelectron. 66 (2015) 527–532.
[23] N. Sui, L. Wang, F. Xie, F. Liu, H. Xiao, M. Liu, H. Xiao, M. Liu, W.W. Yu, Ultrasensitive aptamer-based thrombin assay based on metal enhanced fluorescence resonance energy transfer, Microchim. Acta 183 (2016) 1563–1570.
[24] J. Yang, F. Zhang, Y. Chen, S. Qian, P. Hu, W. Li, Y. Deng, Y. Fang, L. Han, M. Luqman, D. Zhao, Core-shell Ag@SiO_2@ mSiO_2 mesoporous nanocarriers for metal-enhanced fluorescence, Chem. Commun. 47 (2011) 11618–11620.
[25] P. Pompa, L. Martiradonna, A. Della Torre, F. Della Sala, L. Manna, M. De Vittorio, F. Calabi, R. Cingolani, Metal-enhanced fluorescence of colloidal nanocrystals with nanoscale control, Nat. Nanotechnol. 1 (2006) 126.
[26] S.W. Han, W.-G. Koh, Hydrogel-framed nanofiber matrix integrated with a microfluidic device for fluorescence detection of matrix metalloproteinases-9, Anal. Chem. 88 (2016) 6247–6253.
[27] J.-P. Chen, C.-H. Su, Surface modification of electrospun PLLA nanofibers by plasma treatment and cationized gelatin immobilization for cartilage tissue engineering, Acta Biomater. 7 (2011) 234–243.
[28] A. Martins, E.D. Pinho, S. Faria, I. Pashkuleva, A.P. Marques, R.L. Reis, N.M. Neves, Surface modification of electrospun polycaprolactone nanofiber meshes by plasma treatment to enhance biological performance, Small 5 (2009) 1195–1206.
[29] J. Bhadra, N. Al-Thani, S. Karmakar, N. Madi, Photo-reduced route of polyaniline nanofiber synthesis with embedded silver nanoparticles, Arabian J. Chem. (2016), https://doi.org/10.1016/j.arabjc.2016.10.001.
[30] H. Zhang, M. Cao, W. Wu, H. Xu, S. Cheng, L.-J. Fan, Polyacrylonitrile/noble metal/SiO_2 nanofibers as substrates for the amplified detection of picomolar amounts of metal ions through plasmon-enhanced fluorescence, Nanoscale 7 (2015) 1374–1382.
[31] A. González, C. Noguez, J. Beránek, A. Barnard, Size, shape, stability, and color of plasmonic silver nanoparticles, J. Phys. Chem. C 118 (2014) 9128–9136.
[32] S.W. Han, S. Lee, J. Hong, E. Jang, T. Lee, W.-G. Koh, Mutiscale substrates based on hydrogel-incorporated silicon nanowires for protein patterning and microarray-based immunoassays, Biosens. Bioelectron. 45 (2013) 129–135.
[33] K. Ray, J.R. Lakowicz, Metal-enhanced fluorescence lifetime imaging and spectroscopy on a modified SERS substrate, J. Phys. Chem. C 117 (2013) 15790–15797.
[34] A. Shrivastava, V.B. Gupta, Methods for the determination of limit of detection and limit of quantitation of the analytical methods, Chron. Young Sci. 2 (2011) 21.
[35] N. Wang, D. Zhang, X. Deng, Y. Sun, X. Wang, P. Ma, D. Song, A novel surface plasmon resonance biosensor based on the PDA-AgNPs-PDA-Au film sensing platform for horse IgG detection, Spectrochim. Acta, Part A 191 (2018) 290–295.
[36] D. Byrne, Y. Zhao, P. O'Brien, C. McDonagh, Direct spray deposition of silver nanoparticle films for biosensing applications, RSC Adv. 5 (2015) 62836–62843.
[37] E. Jang, K.J. Son, W.-G. Koh, Metal-enhanced fluorescence using silver nanoparticles-embedded polyelectrolyte multilayer films for microarray-based immunoassays, Colloid Polym. Sci. 292 (2014) 1355–1364.
[38] G. Wang, C. Wang, R. Yang, W. Liu, S. Sun, A sensitive and stable surface plasmon resonance sensor based on monolayer protected silver film, Sensors 17 (2017) 2777.
[39] Q. Wang, B.-T. Wang, Surface plasmon resonance biosensor based on graphene oxide/silver coated polymer cladding silica fiber, Sens. Actuators, B 275 (2018) 332–338.
[40] J. Wang, D. Song, L. Wang, H. Zhang, H. Zhang, Y. Sun, Design and performances of immunoassay based on SPR biosensor with Au/Ag alloy nanocomposites, Sens. Actuators, B 157 (2011) 547–553.